Hydrogen Production Characteristics of a Bioethanol Solar Reforming System with Solar Insolation Fluctuations

Shin-ya OBARA

Department of Electrical and Electronic Engineering, Kitami Institute of Technology
165 Koen-cho, Kitami, Hokkaido 090-8507, Japan
E-mail: obara@mail.kitami-it.ac.jp

Abstract

The development of a bioethanol steam reforming system (FBSR) is considered as a means of distributing energy using PEM fuel cells. Small-scale solar collectors (collection areas on the order of several m^2) are installed in a house as a method for applying the FBSR. However, the temperature distribution of a reforming catalyst fluctuates under conditions of unstable solar insolation. Therefore, heat transfer analysis applied in reforming the catalyst layer of the reactor and the temperature distribution and transient response characteristics of the gas composition of the process were investigated. As a case study, meteorological data for representative days in March and August in Sapporo, Japan were recorded, and the hydrogen production speed, power generation output and amount of electricity purchased were analyzed. The results showed that although fluctuations in solar insolation affected the efficiency of the FBSR, the average efficiency of each representative day exceeded 40%. By installing two solar collectors, each with a collection area of 1 m^2, 21% to 25% of the average power demand of an individual house can be supplied.

Keywords: Solar Reforming, Bioethanol, Heat Transfer, Simulation, Hydrogen Production, Solar Radiation

1. Introduction

The thermal efficiency in fuel cells generally depends on the supply method of hydrogen. A large quantity of CO_2 is discharged by reforming systems that use fossil fuels as a heat source and reforming fuel. So, there are researches on much hydrogen production technology using solar energy currently (for example [1-4]). Steam reforming of bioethanol, however, is driven by heat from solar collectors (i.e., a fuel cell system with a bioethanol solar reforming system, or FBSR) [5-7]. We have previously proposed the production characteristics of a domestically installed reformed gas system [5], and a method for weather prediction using a layered neural network [6-7]. FBSR operation results in hydrogen production, which results from supplying ethanol/water vapour to a reforming catalyst layer. The fuel conversion rate depends on the temperature of the catalyst layer and the space velocity of the ethanol/water vapour. Furthermore, the temperature of the catalyst layer is strongly influenced by solar radiation. If the amount of solar radiation input to the acceptance surface of the FBSR fluctuates sharply over a short-time period, the reforming reaction in the catalyst layer will not fully advance due to a response delay. Therefore, in this paper, the unsteady heat transfer of the catalyst layer installed in the reforming unit is analyzed, and the temperature distribution and transient response characteristics of the composition of process gas are investigated. Next, the hydrogen production characteristics of the FBSR are deduced from the results of this analysis. Furthermore, the output characteristics of the PEM fuel cell are examined. The objective of this study is to clarify the characteristics of hydrogen production, efficiency of the reforming component, and operation method for the FBSR under conditions of short-time solar insolation fluctuation. With this information, we can compare the economic performances and

environmental impacts of photovoltaic and other reforming systems. The efficiency of the reforming component is defined as "the higher heating value of hydrogen / the amount of collection of a solar insolation per day".

2. Fuel cell system with a bioethanol solar reforming system (FBSR)

2.1 System block diagram

Figure 1 (a) shows the power system block diagram of a fuel cell system with a bioethanol solar reformer (FBSR) [4-7]. Two parabolic mirrors (solar collector) with a solar tracking system are introduced into the system. The solar energy obtained by solar collector A is used for vaporization of the bioethanol solution (heat source of a vaporizer unit). The solar energy obtained by solar collector B is used as the heat source for the reforming reaction. In this paper, the collecting areas of solar collectors A and B are set to 1 m^2 (unit area).

2.2 The reformed gas and power system

The molar ratio of steam to ethanol (S/C) of the ethanol fuel supplied to the vaporizer unit from the ethanol tank is set as 3.0. The ethanol solution is evaporated by supplying heat from solar collector A to the vaporizer. The ethanol/water vapour is supplied to the reforming component, shown in Fig. 1 (b). The reforming component consists of solar collector B and the reactor, with the catalyst layer shown in Fig. 1 (c). The reactor of the reforming component generates the reformed gas with high concentrations of hydrogen. A large amount of CO is contained in this reformed gas. Consequently, reformed gas is supplied to the shift and CO oxidation units, and the CO concentration is subsequently reduced. Moreover, because much of the water vapour is contained in the reformed gas,

water is removed using the gas cooler. After completing these processes, the reformed gas is supplied to the PEM fuel cell, and direct-current power is obtained. This power is adjusted using a DC-DC converter, DC/AC converter and inverter. However, when customer demand exceeds power output from the system, power is supplied commercially.

2.3 Reforming component

The reactor shown in Fig. 1 (c) is installed at the focal spot of solar collector B, with diameter D_{cs} and width L_{cs}, in the reforming component, shown in Fig. 1 (b). One of the end faces of the reactor is the acceptance surface of the solar insolation, with area A_{hs}. Ethanol/water vapour is supplied from the heat exchange surface of the reactor. The solar insolation input to the heat exchange surface is supplied directly to the catalyst layer in the reactor. In this paper, the fuel vapour accompanying the reaction supplied to the catalyst layer is described as process gas.

3. Heat transfer analysis

3.1 Reactor model

The reactor shown in Fig. 1 (c) is filled with spherical reforming catalyst several millimetres in diameter. As shown in Fig. 2 (a), all of the walls except the solar insolation acceptance surface in the reactor are heat insulated. Moreover, part of the thermal energy of the solar insolation arrive to the heat exchange surface of the reactor is emitted to the ambient air by convective q_{con} (Eq. (1)) and radiative q_{rad} (Eq. (2)) heat transfer. Solar insolation, except for the aforementioned heat dissipation, is

supplied to the catalyst layer from the heat exchange surface, and is used for reforming via heat conduction between catalyst particles and convection of process gas.

3.2 Reactor

Equation (3) describes the heat convection of the catalyst layer, and it contains the Damkohler correction number Da [8]. The right-hand side of Eq. (3) consists of terms describing the convection and chemical reaction of process gas. Here, Nu, Re and Da are calculated using Eqs. (4) to (6), respectively.

3.3 Reforming reaction

Equation (7) is the reaction formula of steam reforming of ethanol. However, the conversion rate from ethanol to hydrogen depends on the temperature of the catalyst layer and space velocity of the ethanol/water vapour. Therefore in the analysis in this paper, the experimental results of E. Akpan et. al., who investigated steam reforming of ethanol (Fig. 2 (b)) using a commercial catalyst, is applied [9]. Figure 2 (b) shows the relationship between the amount of the catalyst, flow rate of ethanol, temperature of the catalyst layer, and fuel conversion rate. The fuel conversion increases such that the catalyst is highly filled when the temperature is high.

3.4 Analysis model of the catalyst layer

The temperature , coordinates of the radial direction and coordinates of the axial direction of the catalyst layer are given by T, r and x, respectively. Equation (8) is the heat diffusion equation in the catalyst layer. Here, q_r is the amount of endothermals in the catalyst layer, and ρ_c, C_c and λ_c are the density, specific heat

and heat transfer coefficient of the catalyst, respectively; t is the sampling time. The catalyst layer of the cylinder type, shown in Fig. 2 (a), is divided into directions of r and x. These areas are used as elements for the analysis. A two-dimensional model is used in this analysis, and the following assumptions are introduced.

Assumptions used for the analysis

a. The catalyst and process gas are at a local thermal equilibrium.

b. The temperature dependence of the physical-property value is taken into account.

c. The flow velocity of the process gas is uniform in all cross-sections.

d. The pressure loss of process gas is not taken into consideration.

Assumption c. and d. differ from an actual state strictly. However, it is thought that these assumptions have the small influence on heat transmission. Figure 2 (c) shows the division elements $el_{x,r}$ of the catalyst layer. Here, $x = 1, 2, ..., N_x$, $r = 1, 2, ..., N_r$, N_r is the element number of the catalyst layer.

3.5 Heat diffusion equation

Based on assumptions a. to d., described in the previous section, and the boundary conditions of Eqs. (9) to (11), the temperature distribution of the catalyst layer is analyzed using the diffusion equation, Eq. (8). A central finite difference method is introduced into Eq. (8) in this analysis. Equation (12) is the mass flow rate of process gas, and Eqs. (13) and (14) are the boundary conditions. The volume flow rate of the process gas in Eq. (12) is u_g, and ρ_g is the mean density of the process gas. The value of u_0 in Eq. (14) represents the space velocity of the fuel vapour at the entrance of the catalyst layer. This value is calculated by dividing the volume flow rate of the

fuel vapour by the cross section of the catalyst layer. Equation (15) is the value of the endothermals from the reforming reaction. Variables g_g, ψ and H_r in Eq. (15) are the molar flow rate of process gas, conversion and reaction heat, respectively. If the temperature T of the catalyst layer is known, the conversion ψ can be obtained from the characteristics of the catalyst. Because H_r is determined by the reaction described by Eq. (7), if g_g is given, we can calculate the amount of endothermals q_{r} using the reforming reaction (Eq. (7)).

4. Analysis method

4.1 Analysis procedure

The surface temperature T_{hs} of the heat exchange surface of the reactor is first calculated. This is calculated by using the heat capacity of the heat exchange surface, input heat of solar insolation q_{s}, convective heat transfer q_{con}, and heat released by radiative heat transfer q_{rad} (Eqs. (1) and (2)). Since the temperature of the catalyst is low, radiation-heat transfer is considered to be small compared with heat conduction and heat transmission. Influence of the radiation heat transmission is not taken into consideration in this analysis. The temperature distribution ($T_{x,r}$) of the catalyst layer, shown in Fig. 2 (c), is obtained by introducing the calculus of finite differences into Eq. (8). The temperature distribution is analyzed for under boundary conditions (Eqs. (9) to (11)). The Gauss-Seidel method is used for calculating the convergence of the calculus of finite differences. If the temperature distribution $T_{x,r}$ is known, the conversion ($\psi_{x,r}$) of each element will be determined from the relationship between the

conversion and temperature of the catalyst layer (Fig. 2 (b)). According to the value of $\psi_{x,r}$, the amount of endothermals ($q_{r,x,r}$) involved in the reforming reaction of the process gas is obtained from Eq. (15). Moreover, the process gas composition at the outlet of element $el_{x-1,r}$ may be calculated from its composition at the outlet of element $el_{x,r}$. The temperature distribution ($T_{x,r}$) of the catalyst layer is then calculated from these results. This calculation is repeated until the solution converges with that from the diffusion equation (Eq. (8)). For each sample, the convergence solution of $T_{x,r}$ is obtained from the same calculation. If $T_{x,r}$ converges, the distribution of the conversion and gas composition can be determined.

4.2 Efficiency of the reforming component

The rate of the amount of solar radiation obtained by solar collectors A and B, and the higher calorific value of the produced hydrogen, is defined as the efficiency of the reforming component. Equation (16) is the formula for the efficiency of the reforming component.

5. FBSR operation

5.1 System specifications

Here, installation of the FBSR to the individual house in Sapporo City, Japan is described. Table 1 gives the analysis condition of the FBSR used in this case study. The area A_{hs} of the solar insolation acceptance surface (heat exchange surface) of the reactor is 0.005 m^2. The diameter D_{cl} of the catalyst layer is 80 mm, and its width L_{cl} is 60 mm. The supporting structure of the reforming catalyst is made of spherical

alumina, the reactor is filled with the reforming catalyst with an average particle diameter of 3 mm and the packing factor is 0.85. The transmissivity of the heat exchange wall of the reactor is set to 0.9, and the collector efficiency (concentration factor of the solar mirror) of the solar collectors is set to 90%. The heat transfer coefficient h_∞ in Eq. (1) assumes natural convection. Here, h_∞ is set to 10 W/m^{2}K. Moreover, ε_{hs} in Eq. (2) is 0.95. The sampling interval time was 0.01 s and the analysis is calculated for a maximum 600 s.

5.2 Analysis conditions

The length of the element is about 2 mm along the r and x directions of the catalyst layer. The number of elements is $N_x = 30$ and $N_r = 40$ for each direction. The sampling interval is 0.01 s, and analysis takes no longer than 600 s. For the convergence calculation of the diffusion equation shown in Fig. (8), the analysis accuracy is less than 10^{-5}. S/C (molar ratio of steam to ethanol) of the ethanol fuel supplied to the vaporizer was 3.0. For the fuel (ethanol solution) supply referenced in Fig. 2 (b), it was decided that the value (amount of catalysts / ethanol flow rate) of the horizontal axis in the figure should be set to 35000 kg/(kmol/s).

6. Analysis results

6.1 Temperature distribution of the catalyst layer

Figure 3 (a) shows the results of the transient response characteristics of the catalyst layer temperature. In this analysis, after the solar insolation was input into the heat exchange surface of the reactor, 0 s is the time when the maximum temperature of the

surface is stabilized. When the outside air temperature is 293 K, the heat exchange surface temperature, for a solar irradiance at 250 W/m^2, rises to about 500 K. On the other hand, at 1000 W/m^2, the heat exchange surface temperature rises to about 890 K. In Fig. 3 (a), since the solar irradiance is large, it is very sensitive to the temperature distribution of the catalyst layer. This is because the conversion of the ethanol/water vapour increases, and the catalyst temperature in the reactor is high. In each result of Fig. 3 (a), the temperature gradient along the x-axis has not reached zero after 100 s. Since the supply direction of fuel is the same as the supply direction of solar radiation, the temperature gradient of the x-axis direction becomes small.

6.2 Composition of the process gas

Figure 3 (b) shows the process gas composition along the direction of the x axis of the catalyst layer. The molar flow rate of hydrogen is larger than for other gas compositions. The distribution of the molar flow rate of hydrogen, and stable time change as a function of the magnitude of the solar insolation, were input into the reactor. At the time of low solar irradiance, the hydrogen production rate for short-time solar insolation with a lot of fluctuation may result in an unstable production rate. For example, in conditions with less than 10 s of solar insolation fluctuation, the hydrogen production rate does not yield the rated speed (0.008 mol/s) in all areas of the catalyst layer, for a solar irradiance of 250 W/m^2.

6.3 Transient response characteristics of the reactor

Figure 4 shows the transient response characteristics of the hydrogen production rate of the reactor. The period of stability of hydrogen production rate is so short that the

solar irradiance input into the reactor is large, and the hydrogen rate affects the outside temperature. This is because the result of Eqs. (1) and (2) is affected by outside temperature. However, under actual weather conditions, a solar insolation fluctuation interval on the order of tens of seconds appears most often. Therefore, in the following section, the hydrogen production rate of the FBSR is investigated using observed solar irradiance data. This paper uses observed solar irradiance data and outside air temperature from the "Surface-weather-observation 1-minute data, 2007. Sapporo district meteorological observatory, Japan. Meteorological Business Support Center" [10].

6.4 Hydrogen production characteristics based on observed weather data

(1) Observed weather data

Figures 5 (a) and (b) are observed weather data of solar irradiance and outside air temperature for August 23 and March 1, 2007 in Sapporo [10]. Moreover, Fig. 6 shows observed data during daylight hours for each day [10]. Because the characteristics of solar irradiance and outside air temperature in March and August differ greatly, representative days were chosen from these months. The solar irradiance in Figs. 5 (a) and (b) correspond with daylight hours, shown in Fig. 6. The daylight hours is defined in period with direct solar radiation 0.12kW/m^2 or more. The amount of hydrogen production, reforming component efficiency, and operation method of the FBSR are investigated using these data.

(2) The amount of hydrogen production

Figure 7 shows the amount of hydrogen produced during every minute of each representative day. As shown in Figs. 5 (a) and (b), the solar insolation fluctuation from

6:00 to 11:00 differs greatly on each representative day. As a result, the fluctuation frequency of the amount of hydrogen produced on August 23 appears greater than that of March 1. The solar irradiance on the morning of March 1 is stable (Fig. 5 (a)), while the solar insolation fluctuation as a result of clouds was recorded on August 23 (Fig. 5 (b)).

6.5 Solar insolation fluctuation and efficiency of the reforming component

Results for solar irradiance, amount of hydrogen production, and efficiency of the reforming component (Eq. (16)) on each representative day are shown in Table 2. The solar irradiance on the representative day in March is 1.32 times that of the representative day in August. However, the difference in the amount of hydrogen produced is 1.17 times. On the other hand, the efficiency of the reforming component in March was larger than in August (47%, vs. 42%, respectively) [11]. As shown in Figs. 5 (a) and (b), solar insolation fluctuated more in August as compared to March. These figures show that fluctuation of the solar irradiance influences the amount of hydrogen produced by the FBSR. Accordingly, the amount of hydrogen produced and efficiency of the reforming component change with the magnitude of solar insolation fluctuation. Moreover, frequent occurrence of large solar insolation fluctuations is disadvantageous for the efficiency of the reforming component.

6.6 Operational plan for the FBSR

The power usage, when introducing the FBSR into the average individual house in Sapporo, is planned using the analysis results of Figs. 5 to 7.

(1) Power load and purchased power

Sapporo is located in a cold district, and the cooling load of the summer season is not taken into consideration. The heating load of the winter, however, is supplied from the exhaust heat and backup boiler of the system. Therefore, the power load patterns for March and August (Figs. 8 (a) and 9 (a)) show that there is no large difference in power usage. However, as Figs. 5 and 6 show, the solar irradiance and outside air temperature differ greatly for each representative month. Figures 8 (b) and 9 (b) show the amount of electricity produced every minute in the FBSR. Since the power storage equipment is not connected to the FBSR, the production of electricity strongly depends on the characteristics of solar irradiance and outside air temperature for that day. In this analysis, the collection area of solar collectors A and B were set to 1 m^2. The characteristics of the purchased power at this time are given in Figs. 8 (c) and 9 (c). From these results, the load peak at 8:00 in the morning can be cut by using power generated by the FBSR. However, in order to cut the peak around 19:00, it is necessary to use a time-shifted power supply by introducing a battery and hydrogen storage system.

(2) Exhaust gas

Figure 10 shows the minute-by-minute discharge pattern of CO_2 by the FBSR. The CO_2 emissions on March 1 and August 23 are 0.732 kg/Day and 0.854 kg/Day, respectively. The greenhouse-gas-emission-factor for power generation in the "Greenhouse Gas Discharge Calculation Method Investigative Commission Report (Ministry of Environment in Japan, August, 2000)" is 0.378 kg･CO_2/kWh. On the other hand, the CO_2 emissions with the FBSR in March and August were the same: 0.306 kg･CO_2/kWh. Using the FBSR, the amount of greenhouse gas discharge can be reduced by 19%, compared to commercial power.

(3) The utilization rate of renewable energy

As shown in Table 2, the percentage utilization of renewable energy by the FBSR in this paper (where the collecting area of the two solar collectors is 2.0 m^2) is 25.3% in August and 21.4% in March. These efficiencies are advantageous compared with the power generation of a photovoltaic cell. They can be further increased by increasing the utilization rate of renewable energy, which can be done by increasing the collecting area of solar collectors A and B. When increasing the collecting area, it becomes necessary to examine the method of storage of produced hydrogen. Some potential methods for the storage of produced hydrogen include using a hydrogen cylinder and battery (e.g., blocks of broken line in Fig. 1 (a)).

7. Conclusions

The hydrogen production rate, power output, and amount of power purchased for a PEM fuel cell using a bioethanol reforming system (FBSR) were investigated by numerical analysis. In this paper, heat transfer analysis was introduced into the catalyst layer of the reforming component. As a result, the relationship between the supply of solar insolation and hydrogen production rate became clear, and the following conclusions were obtained.

(1) The hydrogen molar flow rate and stability time period of the steam reforming reaction change with the magnitude of solar insolation. Moreover, fluctuations in the amount of solar insolation have large effects on the hydrogen production rate of the FBSR. Accordingly, the efficiency of the reforming component falls due to fluctuations in solar insolation. If the solar insolation fluctuation is mostly on the order of tens of seconds, the reforming reaction may not be able to obtain a stable production rate (rated

speed) of hydrogen, and the amount of hydrogen produced and efficiency of the reforming component will decrease.

(2) When the amount of hydrogen produced by the FBSR was analyzed using meteorological data from Sapporo, Japan on March 1 and August 23, 2007, the efficiency of the reforming component was calculated to be 40% or more on both days. Moreover, the CO_2 emissions on March 1 and August 23, 2007 from the FBSR were 0.732 kg/Day and 0.854 kg/Day, respectively. When the greenhouse gas emission factor for power generation specified in the "Greenhouse Gas Discharge Calculation Method Investigative Commission report (Ministry of Environment in Japan, August, 2000)" is used, the amount of greenhouse gas discharge in the FBSR is 19% lower compared to commercial power.

(3) The percent utilization of renewable energy by the 2-m^2 collecting area of the FBSR was 25.3% in August and 21.4% in March. These efficiencies are superior to the efficiency of power generation in a photovoltaic cell. The efficiency performance of the FBSR can sufficiently compete with a commercial photovoltaic cell.

As uncertainty in this analysis, the difference in assumptions described in section 3.4, the calculation error, the setting performance of each equipment, etc. can be considered. Magnitude of these influences is explained by future study.

Nomenclature

A : Area m^2

C : Specific heat J/(g・K)

D : Diameter m

Da : Modified Damkohler number

el : Catalyst layer element number

g_g : Molar flow rate mol/s

H : Reaction heat J/mol

h : Heat transfer coefficient W/(m^2·h·K)

L : Length, width m

M_e : Mass flow rate of ethanol g/s

M_h : Mass flow rate of hydrogen g/s

N : Number of elements

Nu : Nusselt number

P : Power W

Pr : Prandtl number

Q : Quantity of heat J

q : Heat W

R : Radius m

r : Radial direction of the catalyst layer

Re : Reynolds number

T : Temperature K

t : Sampling time s

u : Flow rate m/s

u_0 : Initial flow rate m/s

x : Axial direction of the catalyst layer

Greek Symbols

α_r : Reaction rate mol/(m^3·s)

χ : Layer of the element

ε : Emissivity

η_s : Reforming component efficiency

λ : Heat conductivity W/(m·K)

ρ : Density g/m^3

ν : Kinetic viscosity m^2/s

σ : Stefan-Boltzmann constant

ψ : conversion rate

Subscripts

c : Catalyst

cf : CO oxidation unit to the cell stack

cl : Catalyst layer

cm : Customer

con : Convective heat transfer

cp : Commercial power

cs : Solar collector

dc : DC-DC converter

fc : Cell stack

g : Process gas

h : The higher calorific value of hydrogen

hs : Heat-supply-surface of the reactor

it : DC-AC converter and inverter

pv : Vaporizer pump

r : Reformer

rad : Radiation

rs : Shift unit reactor

s : Sunlight

sc : CO oxidation unit gas cooler

sg : Gas cooler shift unit

∞ : Ambient air

Acknowledgements

This work was partially supported by a Grant-in-Aid for Scientific Research (C) from JSPS.KAKENHI (20560204).

References

[1] Fernando Fresno, Rocío Fernández-Saavedra, M. Belén Gómez-Mancebo, Alfonso Vidal, Miguel Sánchez, M. Isabel Rucandio, Alberto J. Quejido and Manuel Romero, Solar hydrogen production by two-step thermochemical cycles: Evaluation of the activity of commercial ferrites, International Journal of Hydrogen Energy, Vol. 34, No. 7, (2009), 2918-2924.

[2] Patrice Charvin, Abanades Ste´phane, Lemort Florent, Flamant Gilles, Analysis of solar chemical processes for hydrogen production from water splitting thermochemical cycles, Energy Conversion and Management, Vol. 49, (2008), 1547–1556.

[3] Jörg Petrasch, Aldo Steinfeld, Dynamics of a solar thermochemical reactor for steam-reforming of methane, Chemical Engineering Science, Vol. 62, (2007), 4214–4228.

[4] R.E. Clarke, S. Giddey, F.T. Ciacchi, S.P.S. Badwal, B. Paul, J. Andrews, Direct coupling of an electrolyser to a solar PV system for generating hydrogen, International Journal of Hydrogen Energy, Vol. 34, No. 6, (2009), 2531-2542.

[5] Shin'ya OBARA and Itaru TANNO, Development of Distributed Energy System due to Bio-ethanol PEM Fuel Cell with Solar Reforming, Part 1―Evaluation of Basic Performance, *Transactions of the Society of Heating, Air-Conditioning and Sanitary Engineers of Japan*, 123, (2007), 23-32.

[6] Shin'ya OBARA and Itaru TANNO, Development of Distributed Energy System due to Bio-ethanol PEM Fuel Cell with Solar Reforming, Part 2―High-speed analysis of the operation plan using a neural network, *Transactions of the Society of Heating, Air-Conditioning and Sanitary Engineers of Japan*, 130, (2008), 33-42.

[7] Operation Prediction of a Bioethanol Solar Reforming System Using a Neural Network, Shin'ya OBARA and Itaru TANNO, Journal of Thermal Science and Technology, Vol. 2, No. 2, 2007, 256-267.

[8] Y. Usami, S. Fukusako and M. Yamada, Heat and Mass Transfer in a Reforming Catalyst Bed (Quantitative Evaluation of the Controlling Factor by Experiment), *Transactions of the JSME, Series B*, 67(659), (2000), 1801-1808.

[9] E. Akpan, A. Akande, A. Aboudheir, H. Ibrahim and R. Idem, Experimental, Kinetic and 2-D Reactor Modeling for Simulation of the Production of Hydrogen by the Catalytic Reforming of Concentrated Crude Ethanol (CRCCE) Over a Ni-Based Commercial Catalyst in a Packed-Bed Tubular Reactor, *Chemical Engineering Science*,62(12), (2007), 3112-3126.

[10] Surface-weather-observation 1-minute data, 2007 Sapporo district meteorological observatory, Japan Meteorological Business Support Center, (2008), Tokyo.

[11] Study on a Bioethanol Solar Reforming System with the Solar Insolation Fluctuation in Consideration of Heat Chemical Reaction, Shin'ya OBARA and

Abeer Galal El-Sayed, Journal of Power and Energy Systems, Vol. 3, No. 2, 2009, 321-332.

Equations

$$q_{con} = A_{hs} \cdot h_{\infty} \cdot \left(T_{hs} - T_{\infty}\right) \tag{1}$$

$$q_{rad} = \varepsilon_{hs} \cdot A_{hs} \cdot \sigma \cdot \left(T_{hs}^4 - T_{\infty}^4\right) \tag{2}$$

$$Nu = 9.49 \cdot \left(Re \cdot Pr\right)^{0.516} \cdot \left(D_c / D_{cl}\right)^{1.43} + 27.2 \cdot Da^{0.325} \tag{3}$$

$$Nu = h_g \cdot D_c / \lambda_g \tag{4}$$

$$Re = u_g \cdot D_c / \nu_g \tag{5}$$

$$Da = -\left(H_r \cdot a_r\right) \cdot D_c / \left(\rho_g \cdot u_g \cdot C_g \cdot T_g\right) \tag{6}$$

$$C_2H_5OH + 3H_2O \rightarrow 2CO_2 + 6H_2 - 173\text{kJ/mol} \tag{7}$$

$$\left(\frac{\partial^2 T}{\partial r^2} + \frac{1}{r} \cdot \frac{\partial T}{\partial r} + \frac{\partial^2 T}{\partial x^2}\right) + q_r = \frac{\rho_c \cdot C_c}{\lambda_c} \cdot \frac{\partial T}{\partial t} \tag{8}$$

Boundary conditions

$$\frac{\partial T}{\partial r} = 0 \qquad \text{at} \quad r = R_{cl},\ 0 \le x \le L_{cl} \tag{9}$$

$$-\lambda_c \cdot \frac{\partial T}{\partial x} = q_s - q_{rad} - q_{con} = q_s - \varepsilon \cdot \sigma \cdot \left(T_s^4 - T_{\infty}^4\right) - h \cdot \left(T_s - T_{\infty}\right) \tag{10}$$

at $x = 0,\ 0 \le r \le R_{cl}$

$$\frac{\partial T}{\partial x}=0 \quad \text{at} \quad x=L_{cl}, \quad \frac{\partial T}{\partial r}=0 \quad \text{at} \quad r=0 \tag{11}$$

$$T=T_{\infty} \quad \text{for} \quad t=0$$

$$\frac{\partial}{\partial x}\left(\rho_{\mathrm{g}} \cdot u_{\mathrm{g}}\right)=0 \tag{12}$$

$$\frac{\partial u}{\partial r}=0 \quad \text{at} \quad r=R_{cl}, \quad \frac{\partial u}{\partial x}=0 \quad \text{at} \quad x=L_{cl} \tag{13}$$

$$u=u_0 \quad \text{at} \quad x=0, \quad \frac{\partial u}{\partial r}=0 \quad \text{at} \quad r=0 \tag{14}$$

$$q_{\mathrm{r}}=g_g \cdot \psi \cdot H_r \tag{15}$$

$$\eta_s=\frac{\text{The higher heating value of hydrogen}}{\text{Amount of heat collected per day}}=\frac{Q_h}{Q_A+Q_B} \tag{16}$$

Captions

Fig. 1 PEM fuel cell system with bioethanol-solar-reforming (FBSR)

(a) Block diagram

(b) Reforming component

(c) Catalyst layer installed in the reactor

Fig. 2 Heat transfer analysis

(a) Heat loss from the reactor

(b) Catalyst performance [5)]

(c) Change in the composition of process gas

Fig. 3 Temperature distribution and flow rate of process gas in the catalyst layer.

Outside air temperature 293 K.

(a) Temperature distribution in the catalyst layer.

(b) Flow rate of process gas in the catalyst layer.

Fig. 4 Flow rate of hydrogen production

Fig. 5 Weather observation at one-minute intervals in Sapporo [6)]

(a) March 1, 2007

(b) August 23, 2007

Fig. 6 Weather observation during daylight hours at one-minute intervals [6)]

(a) March 1, 2007

(b) August 23, 2007

Fig. 7　Characteristics of the hydrogen flow rate of the FBSR

(a) March 1, 2007

(b) August 23, 2007

Fig. 8　Analysis results of the operation plan on March 1, 2007.

(a) Power load

(b) Power output from the interconnect device

(c) Purchase power

Fig. 9　Analysis results of operation on August 23, 2007.

(a) Power load

(b) Power output from the interconnect device

(c) Purchase power

Fig. 10　Analysis results for CO_2 emissions.

(a) March 1, 2007

(b) August 23, 2007

Table 1　Analysis condition

Table 2　Analysis results of the FBSR performance

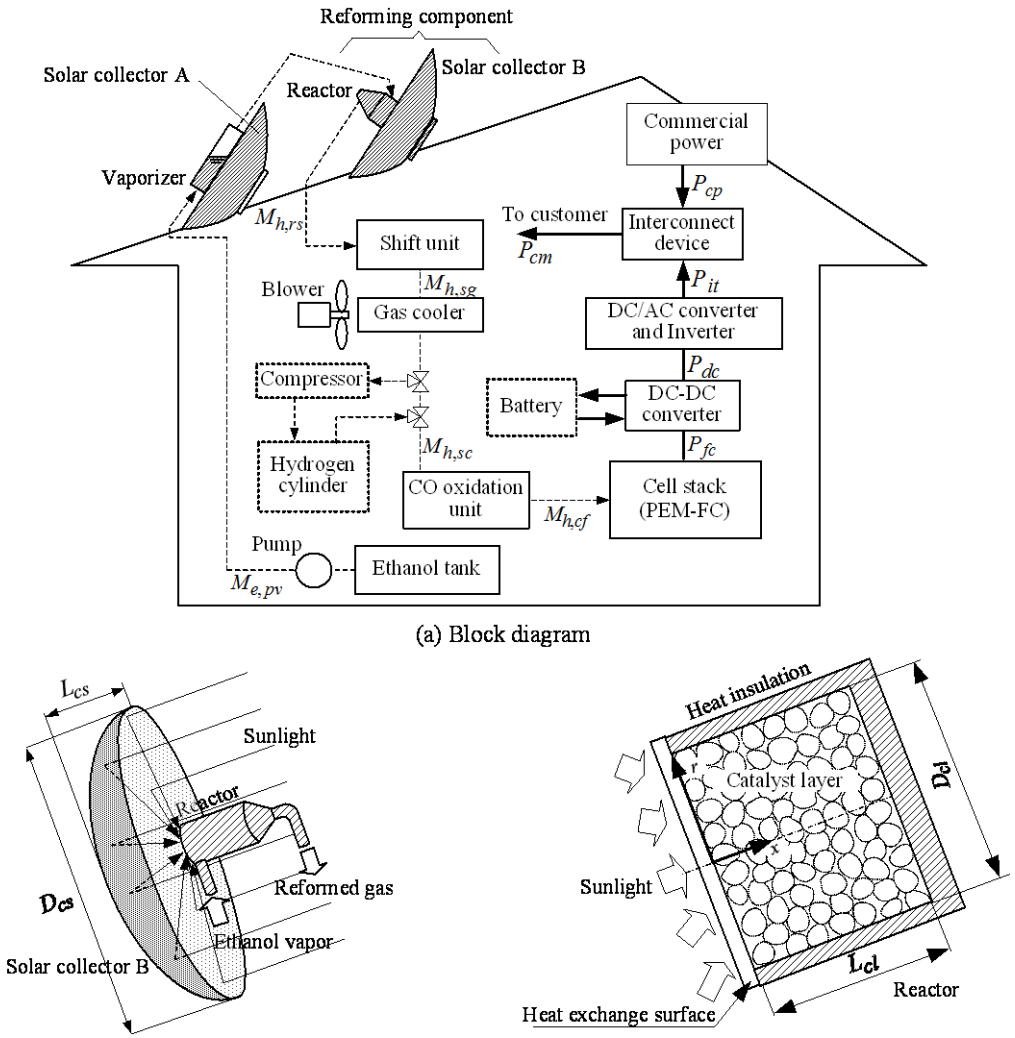

Fig. 1 PEM fuel cell system with bioethanol-solar-reforming (FBSR)

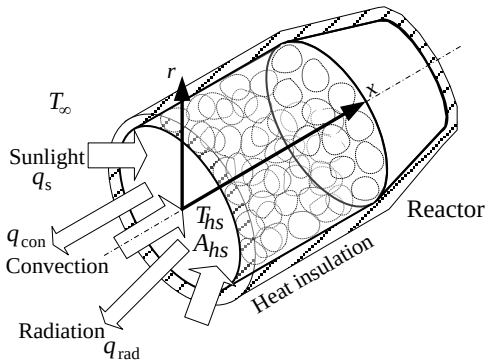

(a) Heat loss from the reactor

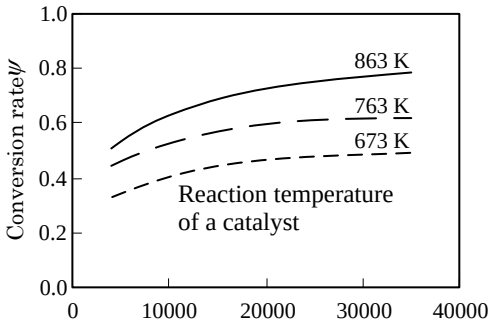

(b) Catalyst performance [5)]

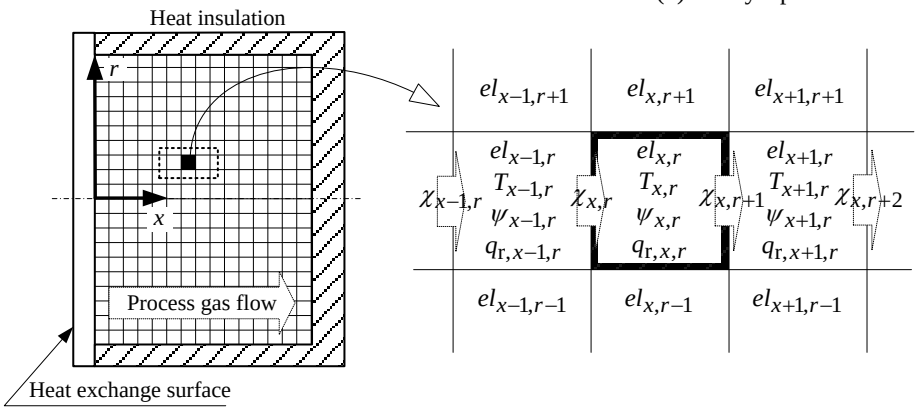

(c) Change in the composition of process gas

Fig. 2 Heat transfer analysis

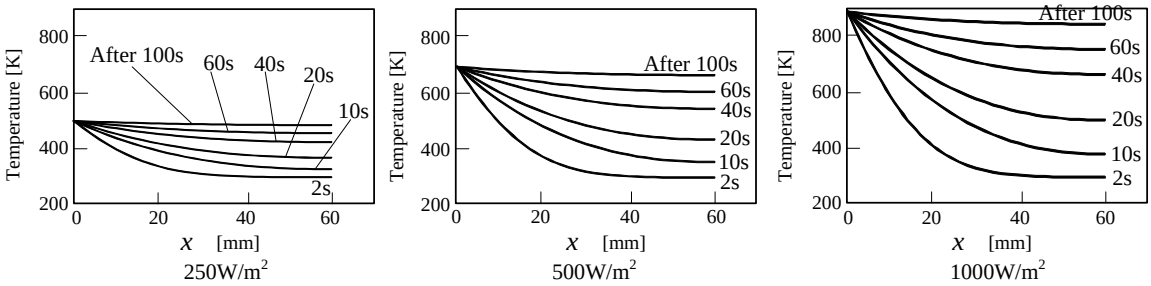

(a) Temperature distribution in the catalyst layer.

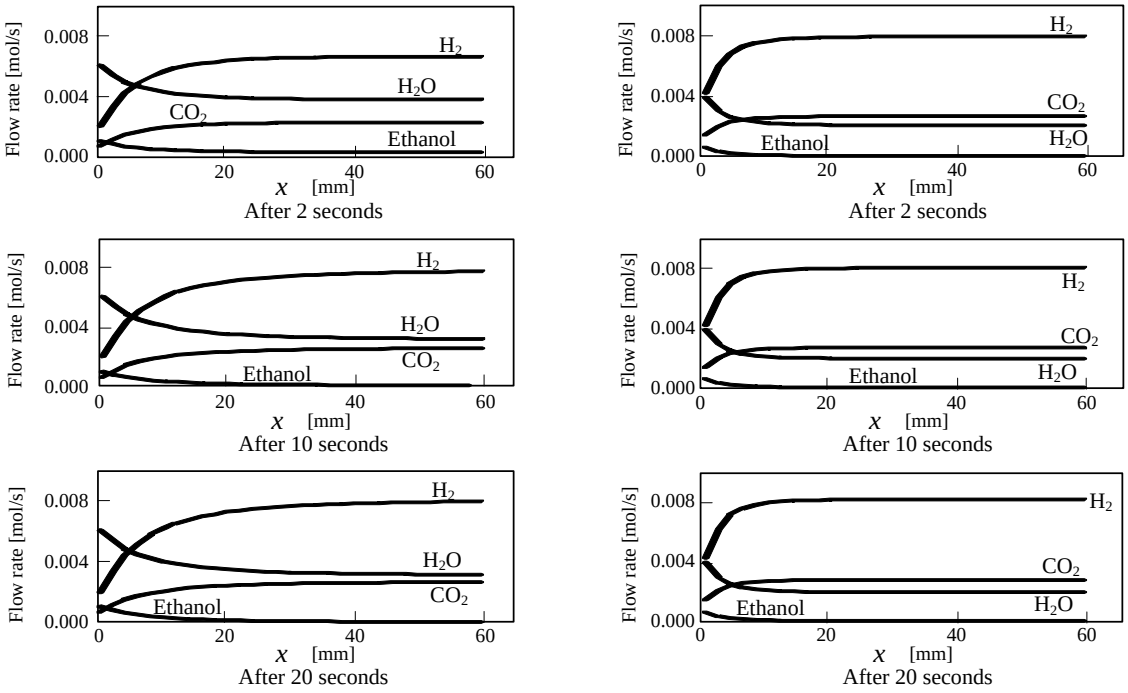

The amount of heat collection by the solar collector B is 250W/m^2 The amount of heat collection by the solar collector B is 500W/m^2

(b) Flow rate of process gas in the catalyst layer.

Fig. 3 Temperature distribution and flow rate of process gas in the catalyst layer. Outside air temperature 293 K.

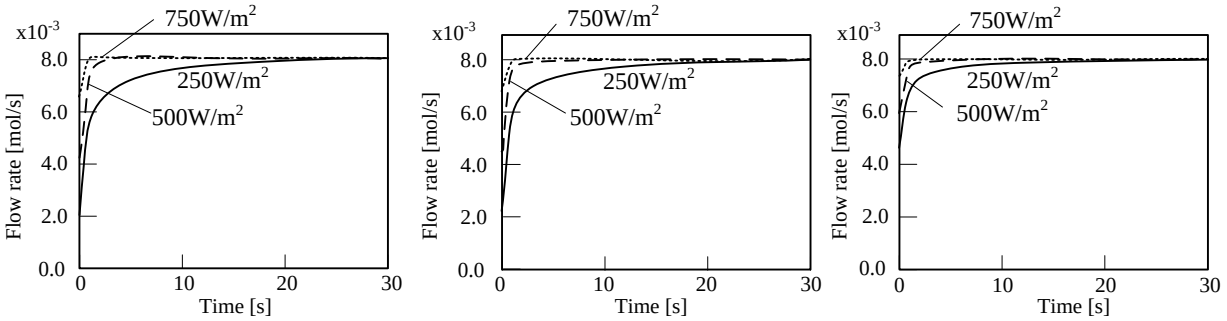

(a) 273 K (b) 293 K (c) 308 K

Outside air temperature

Fig. 4 Flow rate of hydrogen production

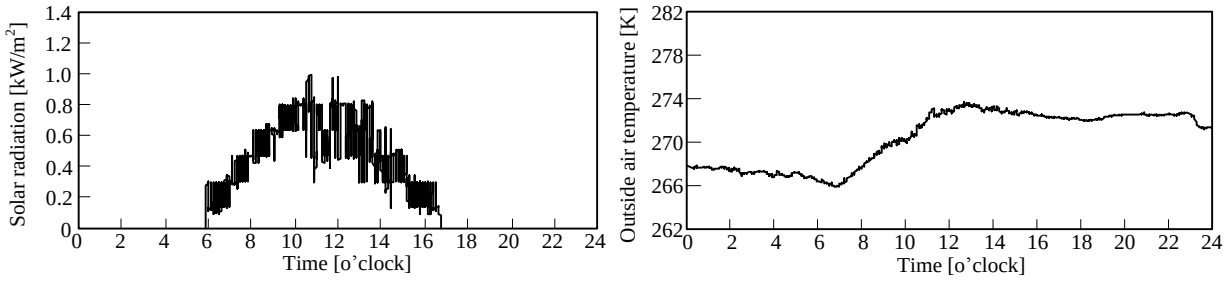

The amount of solar radiation Outside air tmeperature

(a) March 1, 2007

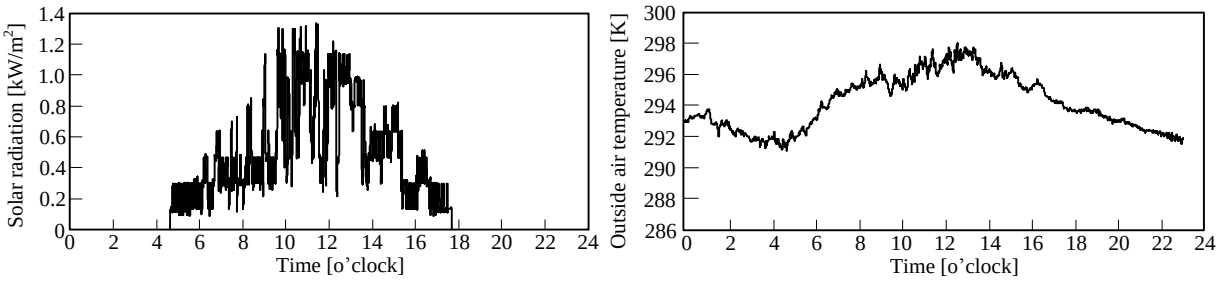

The amount of solar radiation Outside air tmeperature

(b) August 23, 2007

Fig. 5 Weather observation at one-minute intervals in Sapporo [6]

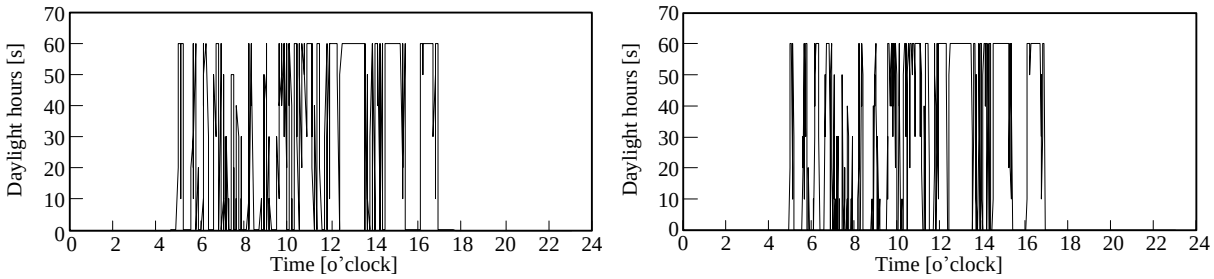

(a) March 1, 2007 (b) August 23, 2007

Fig. 6 Weather observation during daylight hours at one-minute intervals [6]

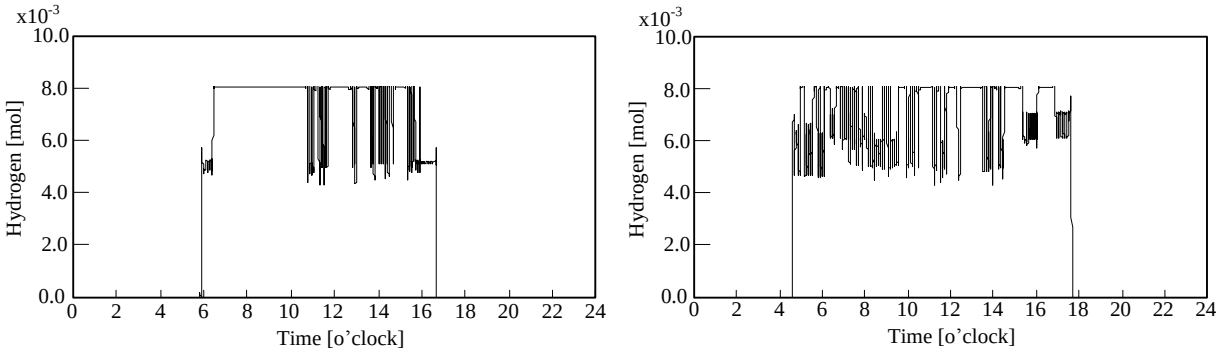

(a) March 1, 2007 (b) August 23, 2007

Fig. 7 Characteristics of the hydrogen flow rate of the FBSR

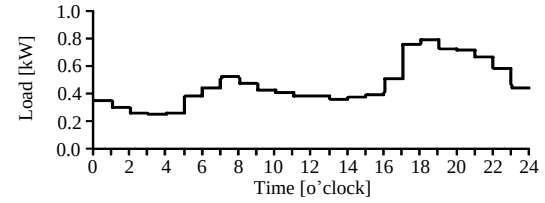

(a) Power load

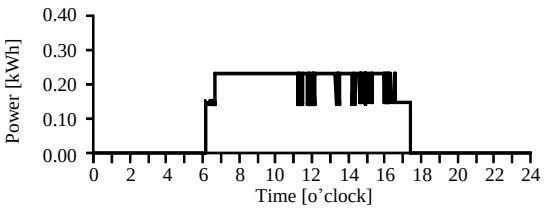

(b) Power output from the interconnect device

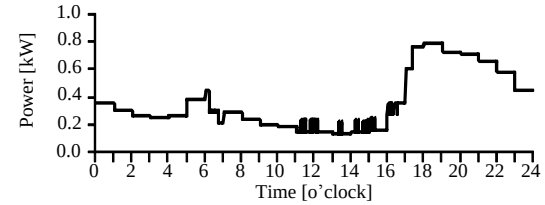

(c) Purchase power

Fig. 8 Analysis results of the operation plan on March 1, 2007.

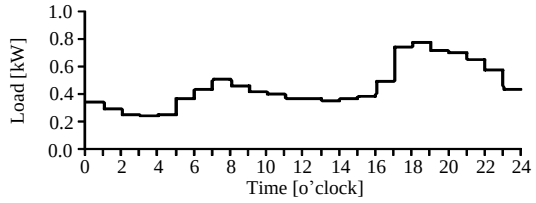

(a) Power load

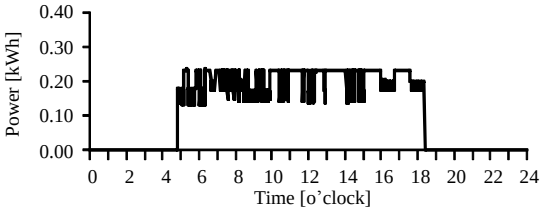

(b) Power output from the interconnect device

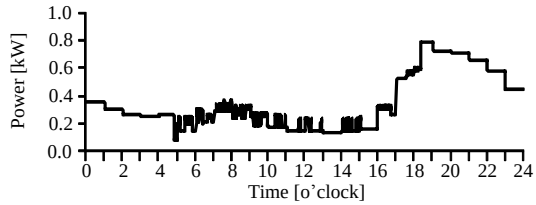

(c) Purchase power

Fig. 9 Analysis results of operation on August 23, 2007.

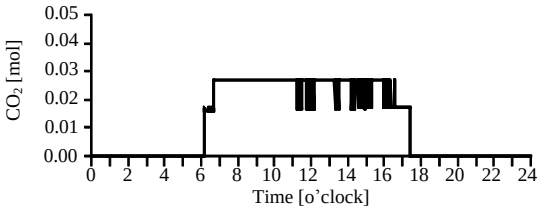

(a) March 1, 2007

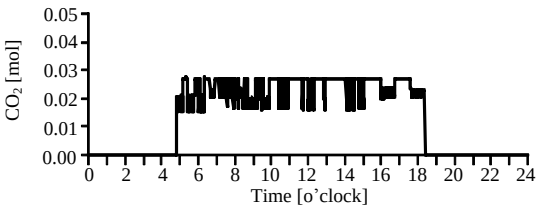

(b) August 23, 2007

Fig. 10 Analysis results for CO_2 emissions.

Table 1 Analysis condition

Concentration area of solar collectors A and B	1.0 m^2
Reactor	
Length of the catalyst layer (L_{cl})	60 mm
Diameter of the catalyst layer (D_{cl})	80 mm
Particle diameter of the catalyst (D_c)	3.0 mm
Steam/carbon ratio	3.0
Catalyst filling factor	0.85
Sampling time	0.01 s
Number of element of *x*-axis (N_x)	30
Number of element of *r*-axis (N_r)	40
Density of the catalyst	213 kg/m^3
Heat conductivity of the catalyst	10 W/mK
Efficiency	
DC-DC converter	95 %
DC-AC converter and inverter	95 %
Loss of the CO oxidation unit	5%

Table 2 Analysis results of the FBSR performance

	March 1	August 23
Daily of solar radiation production for solar collectors A and B	28.0 MJ/Day	37.0 MJ/Day
Amount of hydrogen production per day	100 g/Day	117 g/Day
Efficiency of the reforming component (The higher calorific value of hydrogen / amount of heat collections per day)	47 %	42 %
Amount of daily power demand	11.16 kWh	11.03 kWh
Amount of daily power generation	2.39 kWh	2.79 kWh
Amount of CO_2 emissions per day	732 g/Day	854 g/Day
Renewable energy usage rate (Condensing area 2.0 m^2)	21.4 %	25.3 %